PERGAMON

International Journal of Heat and Mass Transfer 42 (1999) 3279–3290

International Journal of HEAT and MASS TRANSFER

Prandtl number effect on bifurcation and dual solutions in natural convection in a horizontal annulus

Joo-Sik Yoo

Andong National University, Department of Mechanical Engineering Education, 388 Songchun-dong, Andong, Kyungpuk 760-749, South Korea

Received 27 August 1998; received in revised form 17 November 1998

Abstract

Bifurcation phenomena and existence of dual solutions in natural convection in a horizontal annulus are numerically investigated for the fluids of $0.3 \leqslant Pr \leqslant 1$. When the Rayleigh number exceeds a critical value, two kinds of flow patterns are realized: the first is the crescent-shaped eddy pattern in which the fluid in the top of the annulus ascends, and the second is the flow in which the fluid descends by forming two counter-rotating eddies in a half annulus. For the fluids of $0.3 \leqslant Pr \leqslant 0.5$, the second flow pattern can be obtained by the impulsive heating of the inner cylinder, but it is not obtained from the zero initial condition for $0.6 \leqslant Pr \leqslant 1$. The bifurcation points are determined, as a function of the Prandtl number. Hysteresis phenomenon occurs for the fluids of $0.3 \leqslant Pr \leqslant 0.4$, but it is not observed for $0.5 \leqslant Pr \leqslant 1$.

1. Introduction

Natural convection in a horizontal annulus kept at constant surface temperature has been the subject of interest of many researchers due to its theoretical interest and its various engineering applications such as thermal energy storage systems, cooling of electronic components and transmission cables. The basic flow field for low value of Ra forms two symmetric crescent-shaped eddies in which fluid rises near the inner hotter cylinder and sinks near the outer colder one. At high Ra, however, several kinds of convective flows which are dependent on Pr and aspect ratio can be developed. Powe et al. [1,2] and Rao et al. [3] investigated flow patterns of air ($Pr \approx 0.7$), and found three flow regimes depending on diameter ratio (D_i/L): a two-dimensional oscillatory flow for $D_i/L < 2.8$, a three-dimensional spiral flow for $2.8 < D_i/L < 8.5$, and a two-dimensional multicellular flow for $D_i/L > 8.5$. On the other hand, Cheddadi et al. [4] and Yoo [5] investigated the existence of dual steady states for a fluid of $Pr = 0.7$ by introducing artificial numerical disturbances.

To date, much work has been done for the various kinds of natural convection problem in a horizontal annulus: low Prandtl-number fluids [6–9], transient convection [10], the condition of a constant heat flux at the boundaries [11], and a conjugate problem [12]. However, relatively few studies have been made for the effect of Prandtl number [13–15] and the existence of multiple solutions [4,5]. In particular, systematic investigations on the Prandtl-number dependent flow pattern and bifurcation phenomenon have not been made, except those by Yoo [14,15]. Most of the past research has focused the main attention on the heat transfer at the surface of cylinders [13]. Recently, the present author [14,15] considered the natural convection

E-mail address: jsyoo@anu.andong.ac.kr (J.-S. Yoo)

0017-9310/99/$ - see front matter
PII: S0017-9310(98)00384-6

Nomenclature

D_i	diameter of inner cylinder
g	acceleration of gravity
J	Jacobian
L	gap width of the annulus, $R_o - R_i$
Nu_{cond}	Nusselt number of pure conduction state
Nu_i, Nu_o	local Nusselt numbers at the inner and outer cylinders, respectively
$\overline{Nu_i}$, $\overline{Nu_o}$	mean Nusselt numbers at the inner and outer cylinders, respectively
$\overline{Nu}$	overall Nusselt number, $(\overline{Nu_i} + \overline{Nu_o})/2$
Pr	Prandtl number, ν/κ
Ra	Rayleigh number, $\alpha g(T_i - T_o)L^3/\kappa\nu$
R_i, R_o	radii of the inner and outer cylinders, respectively
r	dimensionless radial coordinate
r_i, r_o	dimensionless radii of the inner and outer cylinders, respectively
r_c	radial coordinate of the center of annular gap, $(r_i + r_o)/2$
t	dimensionless time
T_i, T_o	temperatures at the inner and outer cylinders, respectively
u, v	dimensionless velocity components in the radial and angular directions, respectively.

Greek symbols

α	coefficient of thermal expansion
η	stretched coordinate in the radial direction
θ	dimensionless temperature
κ	thermal diffusivity
ν	kinematic viscosity
ρ_0	mean density
ϕ	angular coordinate
Ψ	dimensionless streamfunction
ω	dimensionless vorticity.

Subscripts

cL	lower critical value for bifurcation
cU	upper critical value for bifurcation.

problem in a narrow horizontal annulus, and investigated the effect of the Prandtl number on the stability of conduction regime and transition of flow patterns. It was observed that the stability of the conduction regime of natural convection in a narrow annulus can be classified into two regimes as a function of the Prandtl number: (i) at $Pr \leqslant 0.2$, the instability sets in as steady or oscillatory flows consisting of multiple like-rotating cells in the vertical section of the annulus: (ii) at $Pr \geqslant 0.3$, the instability first sets in at the top part of the annulus. After the onset of the instability, very complex multicellular flow patterns, bifurcation phenomena, and diverse multiple solutions were observed, which were dependent on Pr.

A horizontal annulus with a heated inner cylinder is an interesting physical system, since hydrodynamic instability can occur in the vertical section [16] at low Pr, and Rayleigh–Bénard thermal instability [17] can occur on the top part of the thermally unstable region at high Pr. For the narrow-gap annulus [14,15], it was shown that the Prandtl number plays an important role in the natural convection phenomena, and various transition phenomena depending on Pr were observed.

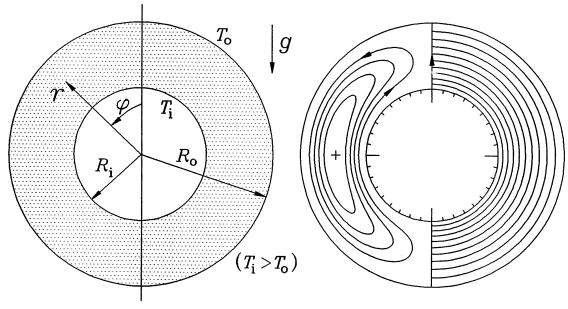

Fig. 1. Problem configuration and a plot of streamlines and isotherms of conduction-dominated regime.

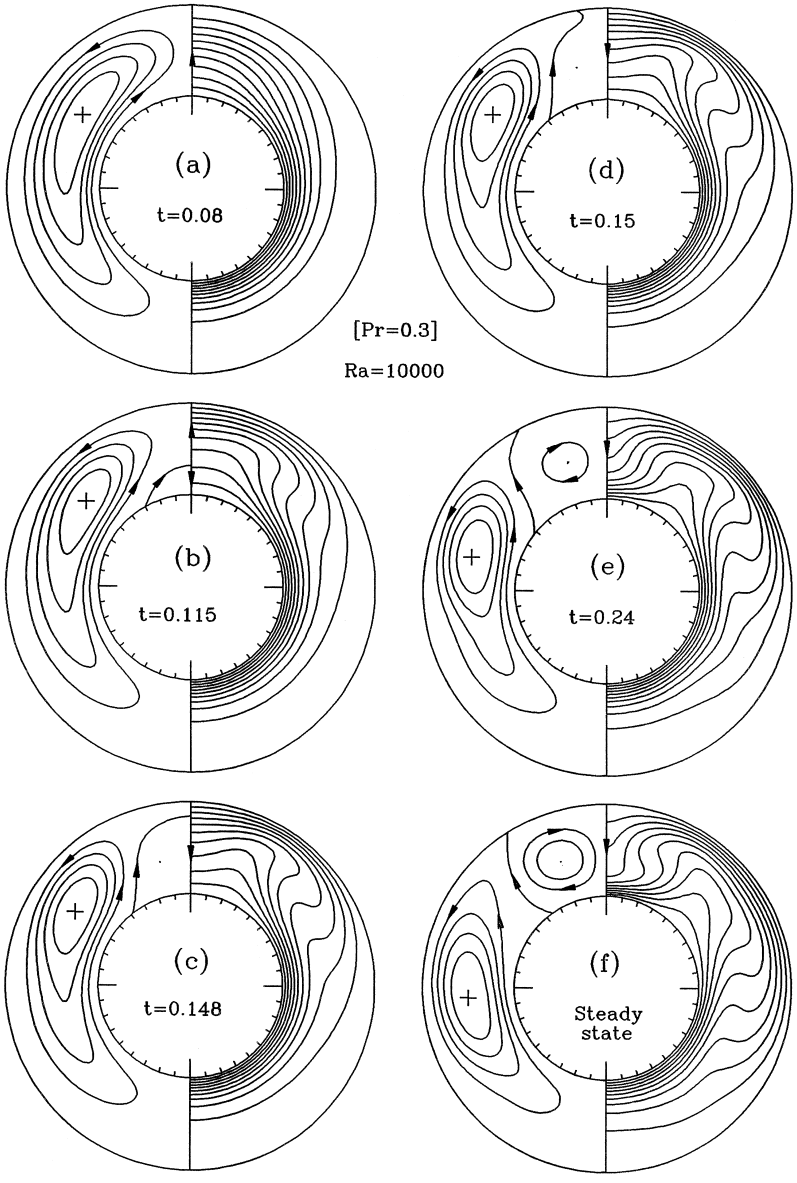

Fig. 2. Transient development of flow patterns for $Pr=0.3$ and $Ra=10^4$: at (a) $t=0.08$; (b) $t=0.115$; (c) $t=0.148$; (d) $t=0.15$; (e) $t=0.24$; (f) steady state. The initial conditions are $\vec{u}=\theta=0$, and the inner cylinder is suddenly heated to $\theta=1$. The cross in the streamfunction field indicates the point of Ψ_{max}.

In this study, we investigate the flow patterns and the bifurcation phenomena for the fluids of $0.3 \leqslant Pr \leqslant 1$, in a wide-gap annulus of $D_i/L=2$. It is found that when Ra exceeds a critical value, two kinds of flow patterns are realized according to initial conditions, and two kinds of bifurcation phenomena are observed, which are dependent on the Prandtl number.

2. Analysis

The geometry of the problem and the coordinate system are shown in Fig. 1. The fluid is contained between two infinite horizontal concentric circular cylinders, which are held at different uniform temperatures of T_i and T_o. The two-dimensional dimensionless

governing equations under Boussinesq approximation can be written as follows [14]:

$$\frac{\partial \omega}{\partial t} = J(\Psi,\omega) + Pr\nabla^2\omega - PrRa\left[\sin(\phi)\frac{\partial \theta}{\partial r} + \cos(\phi)\frac{\partial \theta}{r\partial \phi}\right] \quad (1)$$

$$\omega = -\nabla^2\Psi \quad (2)$$

$$\frac{\partial \theta}{\partial t} = J(\Psi,\theta) + \nabla^2\theta. \quad (3)$$

And the boundary conditions on the two walls are

$$\Psi = \frac{\partial \Psi}{\partial r} = 0, \quad \omega = -\frac{\partial^2\Psi}{\partial r^2}, \quad \theta = 1 \text{ at } r = r_i \quad (4)$$

$$\Psi = \frac{\partial \Psi}{\partial r} = 0, \quad \omega = -\frac{\partial^2\Psi}{\partial r^2}, \quad \theta = 0 \text{ at } r = r_o. \quad (5)$$

In the azimuthal direction, we impose the following symmetric conditions about the vertical plane through the center of cylinders

$$\Psi = \omega = \frac{\partial^2\Psi}{\partial \phi^2} = \frac{\partial \theta}{\partial \phi} = 0 \text{ at } \phi = 0,\pi. \quad (6)$$

The dimensionless heat transfer rate of pure conduction in the absence of fluid motion is

$$Nu_{cond} = \frac{1}{\ln(r_o/r_i)}. \quad (7)$$

And the local Nusselt number is defined as the actual heat flux divided by Nu_{cond}.

$$Nu_i(\phi) = -\left(r\frac{\partial \theta}{\partial r}\right)/Nu_{cond} \text{ at } r = r_i \quad (8)$$

$$Nu_o(\phi) = -\left(r\frac{\partial \theta}{\partial r}\right)/Nu_{cond} \text{ at } r = r_o. \quad (9)$$

Eqs. (1)–(5) are solved by the same finite difference method described in [14]. We use the $(r \times \phi)$ meshes of (45×65) or (65×65). The time step Δt was taken in the range of $10^{-5} \leqslant \Delta t \leqslant 10^{-3}$.

3. Results and discussion

Computations were performed for the fluids with $0.3 \leqslant Pr \leqslant 1$, and an annulus of $D_i/L = 2$ was mainly considered. In the results presented below, the relative gap width is $D_i/L = 2$, unless otherwise mentioned.

The fluid flow for low values of Ra forms a crescent-shaped eddy in which fluid rises near the inner hotter cylinder and sinks near the outer colder one (Fig. 1). In the flow of Fig. 1, the fluid in the top of the annulus ($\phi = 0$) ascends, and we will name it 'upward flow'. At high Ra, however, a flow pattern in which the fluid in the top of the annulus ($\phi = 0$) descends by forming two counter-rotating eddies in a half annulus exists (Fig. 2(f)), and we name it 'downward flow'.

At first, the results for $Pr = 0.3$ will be presented. The transient development of downward flow after impulsive heating of the cylinder is shown in Fig. 2 with $Ra = 10^4$. The initial conditions are $\vec{u} = \theta = 0$, and the inner cylinder is suddenly heated to $\theta = 1$. After 1 s, a flow pattern with a crescent-shaped cell is established, and maintained for a while. At the initial stage, the fluid near the inner cylinder ascends along the circumference of the cylinder, and the boundary layer at the inner cylinder separates from the wall at the top ($\phi = 0$) of the inner cylinder (Fig. 2(a)). The magnitude of the fluid velocity in the top of the annulus where a buoyant plume is created, is increased with time. As time goes on further, however, the zone of strong convective flow moves downward, and the fluid flow in the top of the annulus becomes weak, and consequently a nearly stagnant zone is formed in that region. As a result, the boundary layer at the inner cylinder is separated from the wall at a point $\phi_S (\neq 0)$ near $\phi = 0$, and a small counter-rotating eddy attached to the inner cylinder is created in the top of the annulus. At the onset of the instability of the crescent-shaped upward flow, the created eddy is very small, and is not clearly visible. We can see the creation of the eddy from the value of Ψ_{min}, since Ψ_{min} is zero for upward flow, and has negative value at the onset of the instability. After the onset of the instability, the separation point is shifted downward, and the size of the eddy becomes large. Fig. 2(b) shows that a strong fluid flow occurs in the region of $20^\circ < \phi < 50^\circ$, but the fluid in the top of the annulus ($0 < \phi < 20^\circ$) is almost stagnant. The strong fluid flow in the region of $20^\circ < \phi < 50^\circ$ separates the boundary layer on the inner cylinder from the wall near $\phi = 30^\circ$, and a small counter-rotating eddy is formed in the top of the inner cylinder. The small eddy grows in size with time and extends to the outer cylinder (Fig. 2(c, d)). The magnitude of the strength of the newly created eddy also increases, and finally, a new flow pattern with a counter-rotating eddy on the top of the annulus is established (Fig. 2(e,f)).

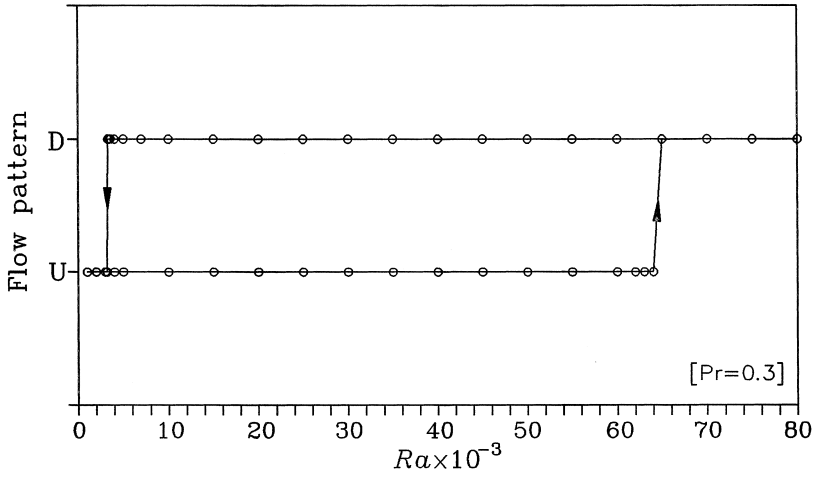

Fig. 3. Bifurcation diagram showing the solution branches found for $Pr=0.3$ in an annulus of $D_i/L=2$. The letters 'U' and 'D' denote the 'upward' and 'downward' flows, respectively.

Fig. 2 shows the separation of the boundary layer on the inner cylinder at a point other than the top of the cylinder ($\phi=0$), which creates an eddy in the thermally unstable top region. Once a small eddy has been created, the eddy grows in size and strength, and finally a downward flow consisting of two counter-rotating eddies develops, if the unstable thermal stratification in the top region is sufficiently strong.

When we start the computation from the zero initial condition, the downward flow is usually obtained for the fluid with $Pr=0.3$, at high Ra. It is observed, however, that if we use the upward flow as an initial condition, the same type of flow pattern is also obtained, at some Rayleigh numbers.

To investigate the above phenomena systematically, Ra was increased starting from $Ra=1000$, and the solution was found by letting the initial condition be the previously obtained (up-scan). And starting from the solution of high Ra with downward flow as an initial condition, the Ra was then sequentially decreased (down-scan). The bifurcation diagram obtained is presented in Fig. 3. The figure shows transitions from downward to upward flow at $Ra_{cL} \approx 3250$ and from upward to downward flow at $Ra_{cU} \approx 6.45 \times 10^4$. We can see a hysteresis phenomenon, and that both upward and downward flows exist at $Ra_{cL} < Ra < Ra_{cU}$. The solutions have been found with the $(r \times \phi)$ mesh of (45×65). We have investigated the effect of grid system. When using 33 and 65 grid points in the ϕ-direction with r-grid points = 25, 35, or 45, the lower critical value of Ra_{cL} was in the range of $3400 < Ra_{cL} < 3500$ and $3200 < Ra_{cL} < 3300$, respectively; and the finer $(r \times \phi)$ mesh of (35×129), yielded Ra_{cL} in the range of $3200 < Ra_{cL} < 3300$.

Examples of dual solutions at $Ra=3300$, 3×10^4, and 6.4×10^4 are presented in Fig. 4. The downward flow consists of a small counter-rotating eddy in the top of the annulus sitting above a large one. In the downward flow, the points of Ψ_{max} and Ψ_{min} indicate the locations of the center of the two cells, and the magnitude of Ψ_{max} and Ψ_{min} represents the relative magnitude of the strength of the cells. For small Ra near the lower critical Rayleigh number (Ra_{cL}), $-\Psi_{min}$ which may be considered as a measure of the strength of the counter-rotating eddy is much smaller than Ψ_{max}. However, the difference becomes small as Ra increases, and at $Ra \geqslant 5.2 \times 10^4$, $-\Psi_{min}$ is greater than Ψ_{max} (Fig. 5(a)). For downward flow, the point of Ψ_{max} which would be the center of the rotation of the large eddy, moves downward as Ra increases, but for upward flow, the point moves upward (Fig. 4).

In the downward flow, the angles (ϕ_S's) which represent the locations of the separation points between the cells on the inner and outer cylinders are plotted in Fig. 5(b) as functions of Ra. The definition of ϕ_S is presented in Fig. 4(b). The approximate size of the counter-rotating cell on the top can be measured from the values of ϕ_S. The angle ϕ_S does not always increase with Ra. Instead, ϕ_S's at the inner and outer cylinders have maximum values at $Ra \approx 7000$ and 4×10^4, respectively. This fact shows a competition between the cells: at the inner cylinder, the upward-driving buoyancy force in the lower cell tends to shift the separation point upward, but the downward-driving force in the upper cell inhibits. Near the lower critical Rayleigh number, the values of ϕ_Ss decrease rapidly as the Rayleigh number decreases, i.e., the counter-rotating cell on the top becomes more and

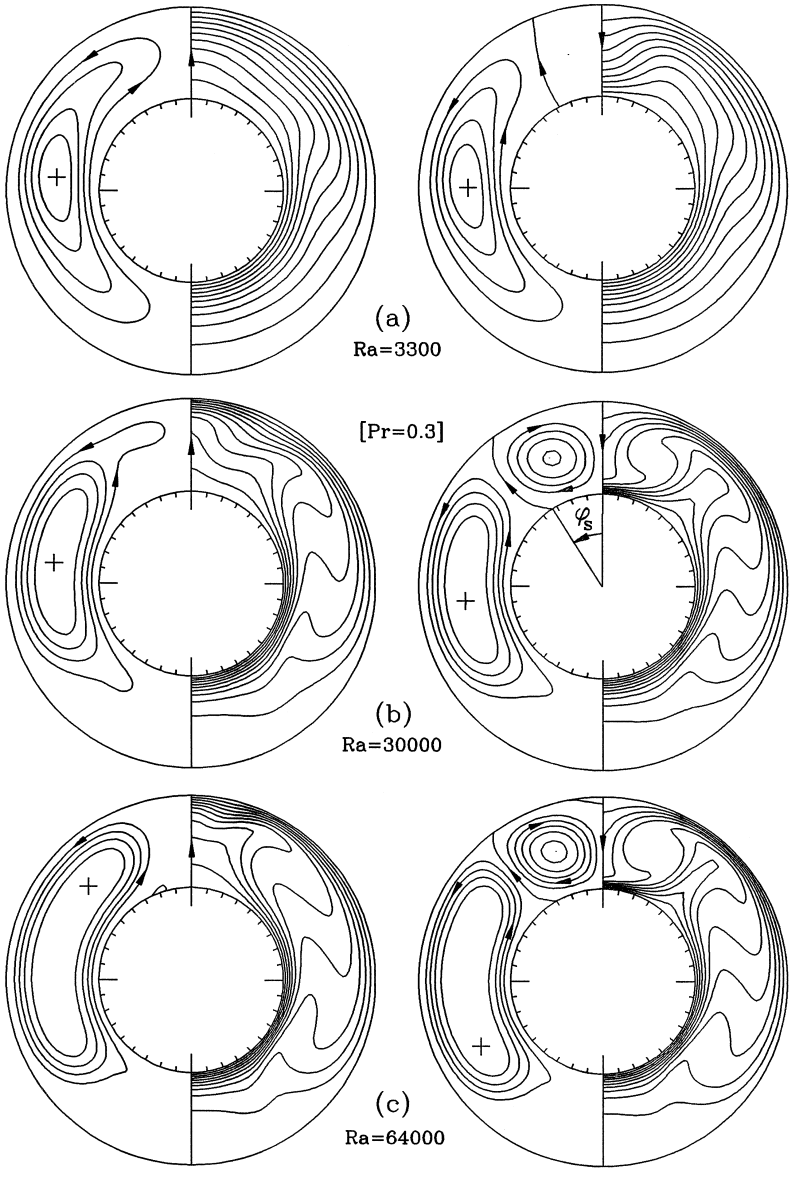

Fig. 4. Streamlines and isotherms of dual solutions for $Pr=0.3$: (a) $Ra=3300$; (b) $Ra=3\times10^4$; (c) $Ra=6.4\times10^4$. The left are upward flows and the right are downward flows.

more slim, and finally it vanishes at Ra_{cL} and the upward flow is established; a transition from downward to upward flow occurs.

The temperature distribution of downward flow differs significantly from that of upward flow, especially in the upper part of the annulus. In Fig. 6, the distributions of local Nusselt numbers at the inner and outer cylinders are presented for $Ra=4000$ and 5×10^4, and the overall Nusselt numbers are shown in Fig. 7 as functions of the Rayleigh number. Apparently, the distributions of local Nusselt numbers for downward flows are different from those of upward flows, except at the bottom region (Fig. 6). Fig. 7 shows that $\overline{Nu}$ of downward flow, $\overline{Nu}$(D), is always greater than that of upward flow, $\overline{Nu}$(U). When $Pr=0.3$, the relative difference of $F=[\overline{Nu}(\mathrm{D})-\overline{Nu}(\mathrm{U})]/\overline{Nu}(\mathrm{U})$ is in the range of $0.12\leqslant F\leqslant0.17$ at $Ra\geqslant10^4$.

In the above, dual solutions for a wide-gap annulus of $D_i/L=2$ were presented, and the solutions have been found even for the wider gap annulus of $D_i/L=0.5$ and 1. One example is presented in Fig. 8 for $D_i/L=0.5$. For $Pr=0.3$, the lower critical Rayleigh

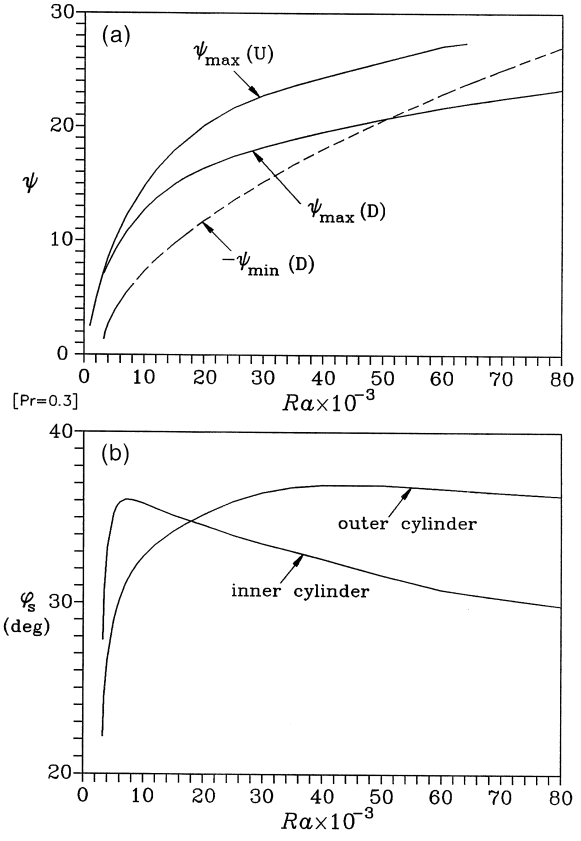

Fig. 5. (a) Maximum and minimum values of streamfunction as functions of Rayleigh number for $Pr=0.3$: the letters 'U' and 'D' denote the 'upward' and 'downward' flows, respectively. (b) Angles (ϕ_S) representing the locations of the separation points between two cells on the inner and outer cylinders for $Pr=0.3$, in the downward flow: the definition of ϕ_S is in Fig. 4(b).

numbers above which dual solutions exist are in the range of $7700 < Ra_{cL} < 7800$, $4200 < Ra_{cL} < 4300$, and $3200 < Ra_{cL} < 3300$, for $D_i/L=0.5$, 1, and 2, respectively, i.e., Ra_{cL} increases as the gap of the annulus becomes wide.

The bifurcation diagram and characteristics of heat transfer for the fluid with $Pr=0.4$ are similar to those of $Pr=0.3$ shown in Figs. 3 and 7. When $Pr=0.4$, the transitions from downward to upward and from upward to downward flow occur at $3050 < Ra_{cL} < 3100$ and $9\times10^4 < Ra_{cU} < 9.5\times10^4$, respectively. The upper critical Rayleigh number (Ra_{cU}) is larger than that of $Pr=0.3$.

For the fluid with $Pr=0.5$, both the upward and downward flows are found at $Ra \geqslant 3000$. One example is presented in Fig. 9 with $Ra=3\times10^4$, and the overall Nusselt numbers as functions of Ra are in Fig. 10. The flow field of $Pr=0.5$ in Fig. 9 and that of $Pr=0.3$ in Fig. 4(b) show that the point of Ψ_{max} is shifted upward with increase of Pr. Unlike the case of $Pr=0.3$ and 0.4, the transition from the solution branch of upward flow to that of downward flow does not occur, when $Pr=0.5$. Computations were carried out up to $Ra=2\times10^5$, but the transition has not been observed. Only the transition from downward to upward flow occurs with decrease of Ra. The overall Nusselt number of downward flow is greater than that of upward flow (Fig. 10), and the relative difference of $F=[\overline{Nu}(D)-\overline{Nu}(U)]/\overline{Nu}(U)$ for $Pr=0.5$ is in the range of $0.09 \leqslant F \leqslant 0.12$ at $Ra \geqslant 10^4$, which is smaller than that of $Pr=0.3$.

When $0.3 \leqslant Pr \leqslant 0.5$, the downward flow can be obtained from the zero initial condition of $\vec{u}=\theta=0$, at high Ra, that is, the transient development of flows after impulsive heating of the inner cylinder yields downward flow naturally for the fluids of $0.3 \leqslant Pr \leqslant 0.5$. At $Pr \geqslant 0.6$, however, the downward flow has not been obtained from the zero initial condition. Contrary to the case of $0.3 \leqslant Pr \leqslant 0.5$, the ascending fluid flow in the top part of the annulus is strong, and a stagnant zone is not formed in that region. Consequently, the boundary layer at the inner cylinder is not separated at a point other than $\phi=0$, and the crescent-shaped upward flow is maintained. However, if we use the downward flow of $0.3 \leqslant Pr \leqslant 0.5$ as an initial condition, the same type of solution is also obtained for $Pr \geqslant 0.6$, at above a certain critical Rayleigh number.

The two types of flows obtained for $Pr=0.7$ with $Ra=10^4$ and 8×10^4 are presented in Fig. 11, in which the left represent the crescent-shaped upward flows which are commonly observed in the numerous previous studies [18]. When $Pr=0.7$, the point of Ψ_{max} moves upward as Ra increases, for both the downward and upward flows. The downward flow exists at $Ra \geqslant 2900$. At $Ra \leqslant 2800$, only upward flow is obtained regardless of the initial conditions. The bifurcation phenomenon for $Pr=0.7$ is similar to that of $Pr=0.5$ in Fig. 10: the transition from downward to upward flow occurs with the decrease of Ra, but the transition from upward to downward flow does not occur. As Ra is increased, the intensity of the buoyant plume directed upward at the top of the annulus ($\phi=0$) becomes more and more strong (Fig. 11), and consequently the transition from upward and downward flow does not occur. The overall Nusselt number of downward flow is greater than that of upward flow, as the case of $Pr=0.3$ and 0.5. The relative difference of $F=[\overline{Nu}(D)-\overline{Nu}(U)]/\overline{Nu}(U)$ for $Pr=0.7$ is in the range of $0.08 \leqslant F \leqslant 0.1$ at $Ra \geqslant 10^4$; and from the results of $\overline{Nu}$ for $Pr=0.3$, 0.5, and 0.7, we can see that the difference of $\overline{Nu}$ between downward and upward flows decreases as Pr increases.

As mentioned above, a transition from upward to downward flow occurs for $Pr=0.3$, but does not for $Pr=0.7$. To see the characteristics of the upward flows

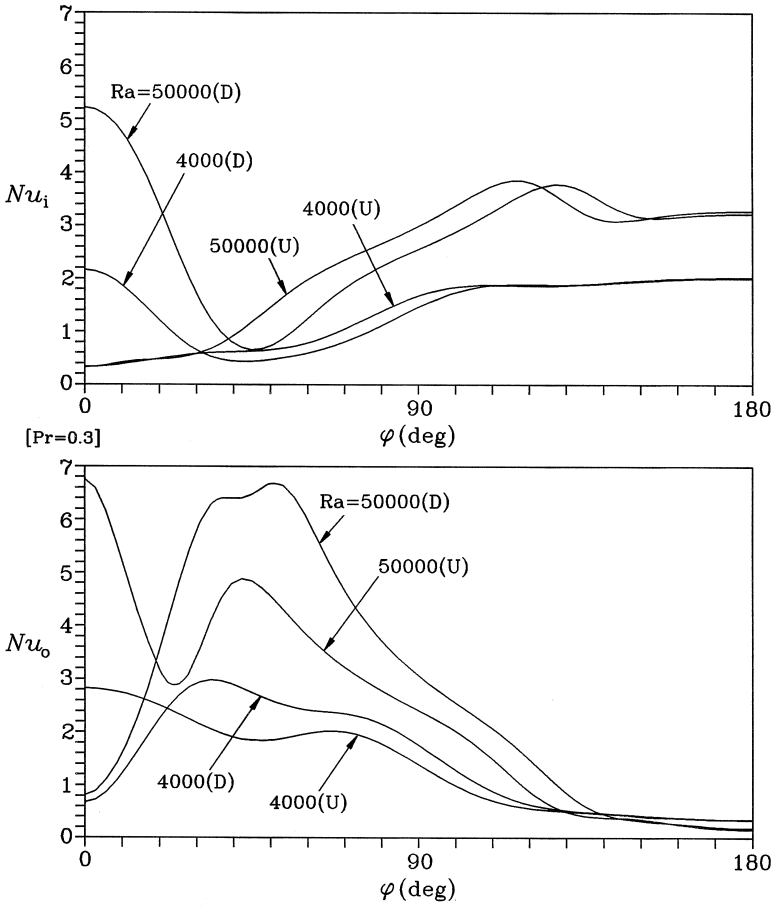

Fig. 6. Distribution of local Nusselt numbers at the inner and outer cylinders for $Pr=0.3$ with $Ra=4000$ and 5×10^4. The letters 'U' and 'D' denote the 'upward' and 'downward' flows, respectively.

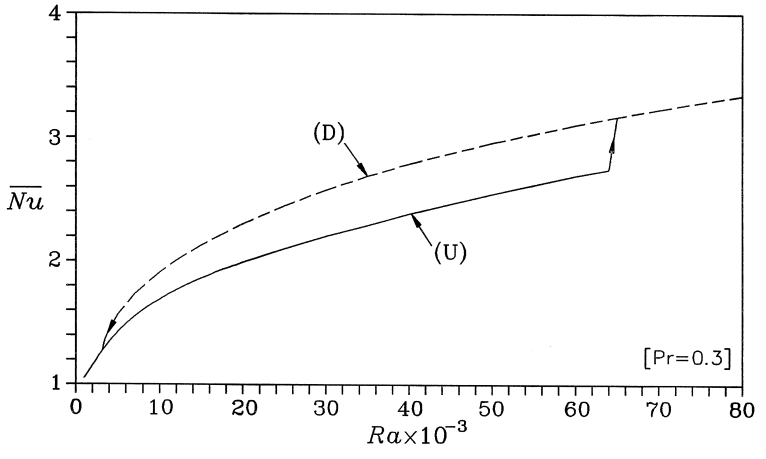

Fig. 7. Overall Nusselt number ($\overline{Nu}$) for $Pr=0.3$. The letters 'U' and 'D' denote the 'upward' and 'downward' flows, respectively.

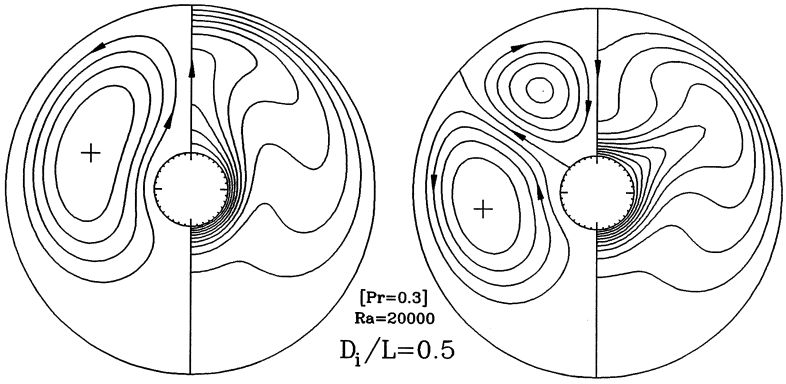

Fig. 8. Streamlines and isotherms of dual solutions in an annulus of $D_i/L=0.5$ with $Pr=0.3$ and $Ra=2\times10^4$.

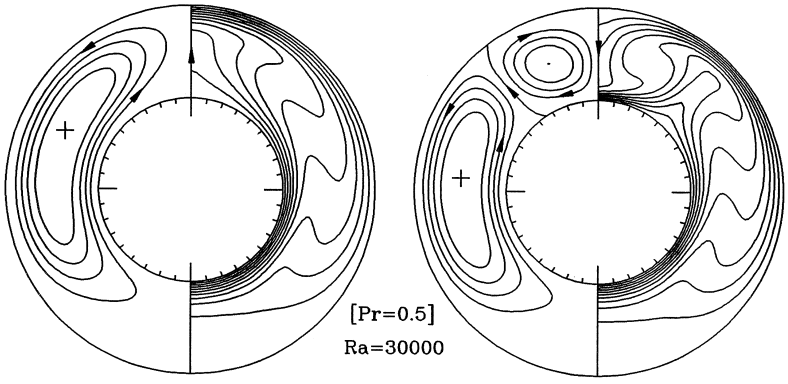

Fig. 9. Streamlines and isotherms of dual solutions for $Pr=0.5$ with $Ra=3\times10^4$.

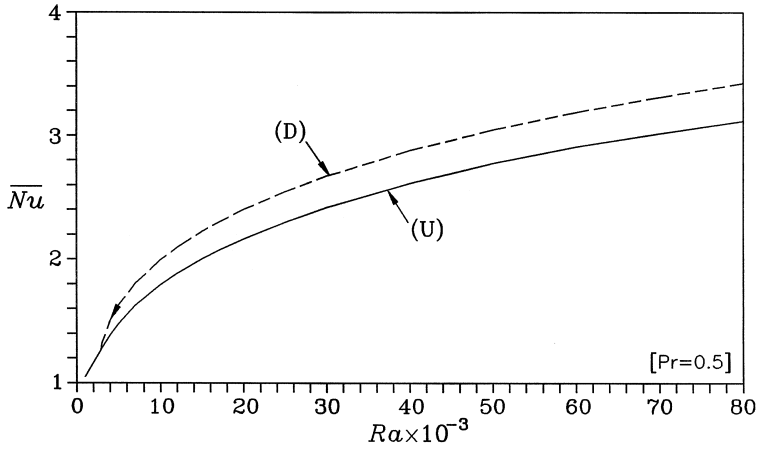

Fig. 10. Overall Nusselt number ($\overline{Nu}$) for $Pr=0.5$. The letters 'U' and 'D' denote the 'upward' and 'downward' flows, respectively.

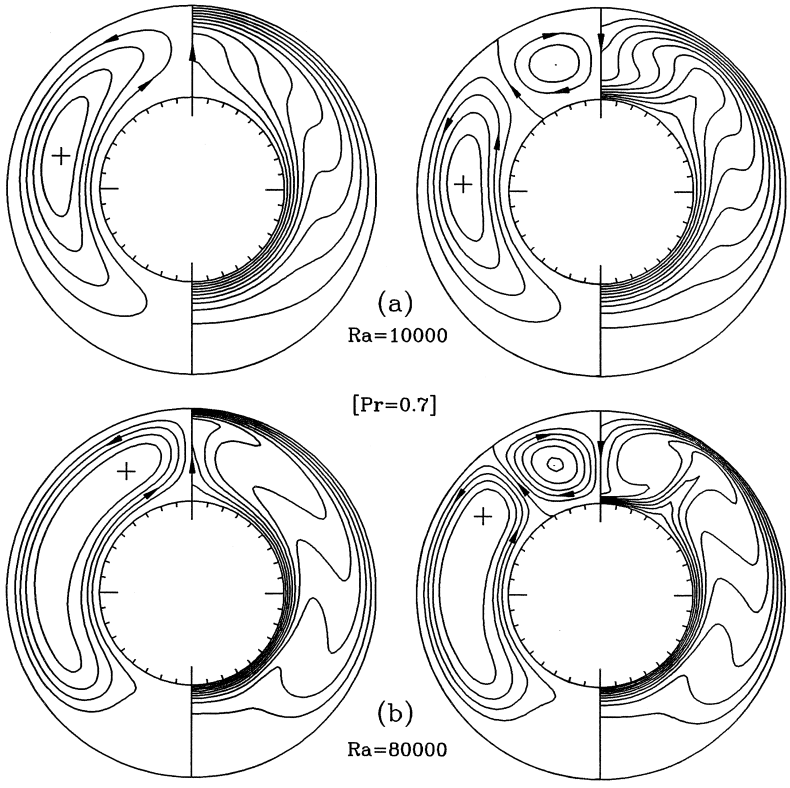

Fig. 11. Streamlines and isotherms of dual solutions for $Pr=0.7$: (a) $Ra=10^4$; (b) $Ra=8\times10^4$.

which yield different transition phenomena for $Pr=0.3$ and 0.7, the distributions of the radial velocity at the centerline of the annular gap, $u(r_c, \phi)$, are presented in Fig. 12 as functions of the Rayleigh number. In the lower part of the annulus ($90^\circ < \phi < 180^\circ$), the velocity profile of $Pr=0.3$ is similar to that of $Pr=0.7$. However, significant different characteristics can be seen in the upper part of the annulus ($0 < \phi < 90^\circ$).

When $Pr=0.3$ (Fig. 12(a)), $u(r_c, \phi)$ has maximum values at the points other than the uppermost point of the annulus ($\phi=0$): the points for $Ra=3000$, 10^4, 2×10^4, 4×10^4, and 6×10^4 are $\phi\approx65$, 57, 50, 34 and 25°, respectively. The velocity at $\phi=0$, $u(r_c, 0)$, does not always increase with Ra. For $Ra=2\times10^4$, 4×10^4, and 6×10^4, $u(r_c, 0)$ is decreased, as Ra increases. It can also be seen that the fluid near the region of $\phi=0$ is nearly stagnant at $Ra=6\times10^4$. On the other hand, the point of maximum velocity is shifted upward and the magnitude of the maximum velocity increases monotonously, as Ra increases. The upward flow pattern is maintained up to $Ra=6\times10^4$. At a critical value of $Ra=6.5\times10^4$, however, the strong fluid flow near the point of the maximum velocity ($15^\circ < \phi < 35^\circ$) separates the boundary layer on the inner cylinder at $\phi_S(\neq0)$, since the fluid in the top of the annulus ($0 < \phi < \phi_S$) is nearly stagnant. As a result a counter-rotating eddy is created on the top of the annulus, and afterwards the fluid flow in the top of the annulus becomes strong, due to the unstable thermal stratification in the upper part of the annulus. And the strength of the counter-rotating eddy increases; a transition from upward to downward flow occurs.

When $Pr=0.7$, Fig. 12(b) shows that $u(r_c, \phi)$ has maximum values at the uppermost point of the annulus ($\phi=0$) for all Rayleigh numbers, i.e., the most strong fluid flow directed upward occurs in the top of the annulus ($\phi=0$), and $u(r_c, 0)$ increases continuously with Ra. Accordingly, the boundary layer on the inner cylinder does not separate from the wall at a point other than $\phi=0$, and the upward flow pattern is maintained always; a transition from upward to downward flow does not occur.

Cheddadi et al. [4] and Yoo [5] investigated dual steady solutions for the fluid with $Pr=0.7$ (air), in which the downward flow (or bicellular flow) was obtained by introducing artificial numerical disturbances. The upper part of an annulus with a heated inner cylinder is thermally unstable, and accordingly, the instability of the crescent-shaped upward flow which yields downward flow can persist, if the unstable

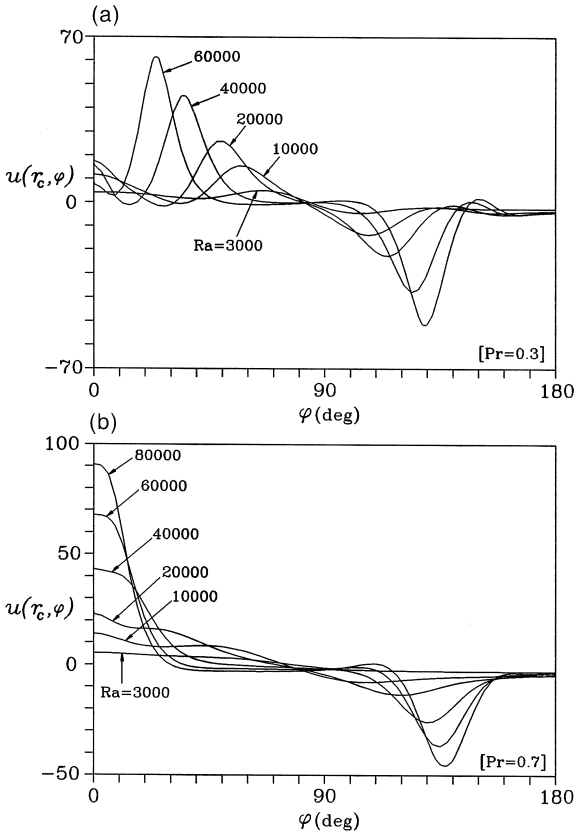

Fig. 12. Distribution of the radial velocity of upward flow at the centerline of the annular gap, as a function of *Ra*: (a) $Pr=0.3$; (b) $Pr=0.7$.

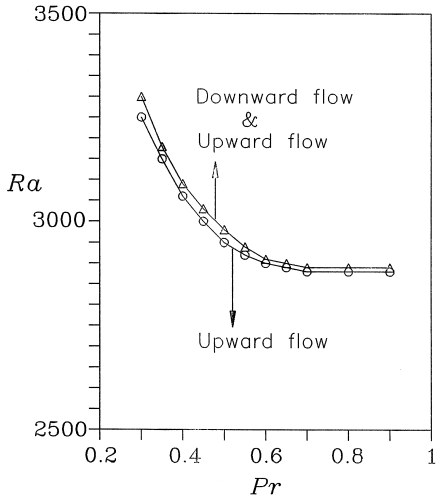

Fig. 13. Map of downward and upward flows on the *Pr*–*Ra* plane, for an annulus of $D_i/L=2$.

stratification in the top region is sufficiently strong. In this study, we have observed that the transient development of flows after impulsive heating of the inner cylinder yields downward flow for the fluids of $0.3 \leqslant Pr \leqslant 0.5$. The natural occurrence of downward flow for $0.3 \leqslant Pr \leqslant 0.5$ may be caused by the combined effect of hydrodynamic and thermal instability; and the downward flow for $Pr=0.7$ was obtained with the solution of $0.3 \leqslant Pr \leqslant 0.5$. When $Pr=0.7$, the critical Rayleigh number above which dual solutions exist is in the range of $2880 < Ra_c < 2890$, which is larger than $Ra_c=1708$ in the Rayleigh–Bénard problem [17]. The characteristics of the dual solutions and the bifurcation phenomenon for $Pr=0.7$ are in accordance with those of Cheddadi et al. [4] and Yoo [5].

Finally, the map of flow regime on the *Pr*–*Ra* plane is presented in Fig. 13. The critical Rayleigh number above which both the upward and downward flows exist is decreased, as *Pr* increases. This is due to the stabilizing effect of viscous force and temperature field in the thermally unstable upper region. Once the thermal plume on the upper part of the annulus has been established, the viscous drag tends to maintain the shape of the thermal plume, and the force is increased with increase of *Pr*.

4. Conclusions

The flow patterns and the bifurcation phenomena in natural convection in a horizontal annulus are numerically investigated for the fluids of $0.3 \leqslant Pr \leqslant 1$. When *Ra* exceeds a critical value, two kinds of flow patterns named 'downward flow' and 'upward flow' which are characterized by the direction of the fluid flow in the top of the annulus, are realized. For the fluids of $0.3 \leqslant Pr \leqslant 0.5$, the transient development of flows after impulsive heating of the inner cylinder yields downward flow. At $0.6 \leqslant Pr \leqslant 1$, however, the downward flow has not been obtained from the zero initial condition. At the onset of the instability of upward flow, a nearly stagnant zone is formed in the top part of the annulus, and the boundary layer on the inner cylinder separates from the wall at a point other than the top of the cylinder. At $0.3 \leqslant Pr \leqslant 0.4$, both of the transitions from downward to upward and from upward to downward flow occur. When $0.5 \leqslant Pr \leqslant 1$, however, only the transition from downward to upward flow occurs with decrease of *Ra*. The characteristics of upward flow which determine the transition phenomenon are elucidated by the distributions of radial velocity at the centerline of the annular gap. As *Pr* increases, the critical Rayleigh number above which both of the upward and downward flows exist is decreased. The temperature distribution of downward flow differs significantly from that of upward flow,

except at the lower part of the annulus. The overall Nusselt number of downward flow is greater than that of upward flow, and the difference decreases, as Pr increases.

References

[1] R.E. Powe, C.T. Carley, E.H. Bishop, Free convective flow patterns in cylindrical annuli, Journal of Heat Transfer 91 (1969) 310–314.

[2] R.E. Powe, C.T. Carley, S.L. Carruth, A numerical solution for natural convection in cylindrical annuli, Journal of Heat Transfer 93 (1971) 210–220.

[3] Y.F. Rao, Y. Miki, K. Fukuda, Y. Takata, S. Hasegawa, Flow patterns of natural convection in horizontal cylindrical annuli, International Journal of Heat and Mass Transfer 28 (1985) 705–714.

[4] A. Cheddadi, J.P. Caltagirone, A. Mojtabi, K. Vafai, Free two-dimensional convective bifurcation in a horizontal annulus, Journal of Heat Transfer 114 (1992) 99–106.

[5] J.-S. Yoo, Dual steady solutions in natural convection between horizontal concentric cylinders, International Journal of Heat and Fluid Flow 17 (1996) 587–593.

[6] L.R. Mack, E.H. Bishop, Natural convection between horizontal concentric cylinders for low Rayleigh numbers, Quarterly Journal of Mechanics and Applied Mathematics 21 (1968) 223–241.

[7] J.R. Custer, E.J. Shaughnessy, Thermoconvective motion of low Prandtl number fluids within a horizontal cylindrical annulus, Journal of Heat Transfer 99 (1977) 596–602.

[8] M.C. Charrier-Mojtabi, A. Mojtabi, J.P. Caltagirone, Numerical solution of a flow due to natural convection in horizontal cylindrical annulus, Journal of Heat Transfer 101 (1979) 171–173.

[9] J.-S. Yoo, J.Y. Choi, M.-U. Kim, Multicellular natural convection of a low Prandtl number fluid between horizontal concentric cylinders, Numerical Heat Transfer, Part A 25 (1994) 103–115.

[10] Y.T. Tsui, B. Tremblay, On transient natural convection heat transfer in the annulus between concentric horizontal cylinders with isothermal surfaces, International Journal of Heat and Mass Transfer 27 (1984) 103–111.

[11] P. Kumar, Study of natural convection in horizontal annuli, International Journal of Heat and Mass Transfer 31 (1988) 1137–1148.

[12] P.M. Kolesnikov, V.I. Bubnovich, Non-stationary conjugate free-convective heat transfer in horizontal cylindrical coaxial channels, International Journal of Heat and Mass Transfer 31 (1988) 1149–1156.

[13] T.H. Kuehn, R.J. Goldstein, A parametric study of Prandtl number and diameter ratio effects on natural convection heat transfer in horizontal cylindrical annuli, Journal of Heat Transfer 102 (1980) 768–770.

[14] J-S. Yoo, Natural convection in a narrow horizontal cylindrical annulus: $Pr \leqslant 0.3$, International Journal of Heat and Mass Transfer 41 (1998) 3055–3074.

[15] J-S. Yoo, Transition and multiplicity of flows in natural convection in a narrow horizontal cylindrical annulus: $Pr = 0.4$, International Journal of Heat and Mass Transfer 42 (1999) 709–722.

[16] Y. Lee, S.A. Korpela, Multicellular natural convection in a vertical slot, Journal of Fluid Mechanics 126 (1983) 91–121.

[17] F.H. Busse, Transition to turbulence in Rayleigh–Bénard convection, in: H.L. Swinney, J.P. Gollub (Eds.), Topics in Applied Physics, vol. 45, Springer-Verlag, 1981, pp. 97–137.

[18] T.H. Kuehn, R.J. Goldstein, An experimental and theoretical study of natural convection in the annulus between horizontal concentric cylinders, Journal of Fluid Mechanics 74 (1976) 695–719.